Journal of Imaging Science and Technology® 54(6): 060503–060503-11, 2010.

Characterization of White Paper Sheets by BRDF Model Parameters Estimated in the Specular Reflection Plane

Yoshinori Akao
National Research Institute of Police Science, 6-3-1 Kashiwanoha, Kashiwa, Chiba 2770882, Japan
E-mail: akao@nrips.go.jp

Norimichi Tsumura and Toshiya Nakaguchi
Graduate School of Advanced Integration Science, Chiba University, 1-33 Yayoi-cho, Inage-ku, Chiba 263-8522, Japan

Yoichi Miyake
Research Center for Frontier Medical Engineering, Chiba University, 1-33 Yayoi-cho, Inage-ku, Chiba 263-8522, Japan

Abstract. *We characterize sheets of white paper using three bidirectional reflectance distribution function (BRDF) model parameters estimated from the BRDF in the specular reflection plane. The radiance factors of eight types of paper sheets having a wide range of material characteristics were measured for 284 geometries in the specular reflection plane. They were approximated within an average error of 4.5% using a linear combination of Torrance-Sparrow and Lambert's BRDF models. The proposed model well approximated the BRDF of samples in the specular plane. Based on the estimated BRDF model parameters, the eight measured paper sheets could be broadly classified into glossy papers and rough papers. The two glossy papers were distinguishable from each other, while the six rough papers could be classified into three groups using the BRDF model parameters. The proposed method is considered to be effective for characterizing a wide range of white paper ranging from glossy to matte paper. © 2010 Society for Imaging Science and Technology.*
[DOI: 10.2352/J.ImagingSci.Technol.2010.54.6.060503]

INTRODUCTION

Identification of paper sheets based on their appearance is both an important skill and a challenging problem. Paper is used extensively in everyday life. There are various types of paper having a range of different material characteristics, including different levels of glossiness and roughness. Quantitative evaluation of the material characteristics of paper is important in the paper and printing industries for assessing the grades of paper, and in machine vision—which promises to replace manual visual inspection of paper. It is also important with respect to archiving historical documents and paintings. Finally, it is crucial in criminal investigations that use evidence based on the forensic analysis of documents such as counterfeit banknotes and security documents, as well as threatening and harassing letters.

The visual aspects of paper sheets are considered to have relationships mainly with their optical properties. Concerning the optical properties of paper sheets, various ISO test standards have been determined, for example whiteness,[1] opacity,[2] color,[3–5] diffuse reflectance factor,[6,7] scattering and absorption coefficient,[8] and specular gloss.[9–11] These standards serve as industrial standards, and they are widely applied to a diverse range of measurement instruments such as a gloss meter. In particular, with respect to the glossiness of paper sheets, the relationship between topography and gloss,[12] and their relationships with the psychological sensory scale have been studied.[13,14] However the measurement geometries are fixed in one direction for these indexes, therefore they may show only one aspect of the optical properties. For example, conventional specular gloss is insufficient to represent the off-specular phenomenon that is frequently observed in paper sheets with rough surfaces.

The bidirectional reflectance distribution function (BRDF)[15] is considered to be essential for the characterization of white paper sheets based on their appearances, as it has the ability to represent various aspects of the optical reflection properties of an object. BRDF represents the optical reflection property of objects as a function of four variables expressed in terms of geometrical coordinates. It describes how an object converts incident illumination into reflected light. The material characteristics of white paper sheets are considered to be strongly related to their BRDF. However, raw BRDF data is complicated when it comes to representing material characteristics, therefore it is necessary to parameterize BRDF by modeling the optical properties of paper sheets.

Concerning the optical modeling of paper sheets, the Kubelka-Munk theory was developed to describe the propagation of light in turbid media.[16,17] Since its introduction in the 1930s, several modifications have been made to the Kubelka-Munk theory to extend its applicability. Kubelka-Munk theory is convenient in that it provides an analytical solution. However, it does not describe BRDF, as the only

Received Aug. 19, 2009; accepted for publication Jul. 6, 2010; published online Nov. 5, 2010.
1062-3701/2010/54(6)/060503/11/$20.00.

directional information it gives is in the upward or downward directions. Another approach was developed based on radiative transfer theory,[18] which introduces phase functions such as Henyey-Greenstein phase functions.[19] Angle-dependent light scattering distributions were generated by introducing multi-flux theory, which solves the radiative transfer equation by splitting the directional information into multiple channels.[20,21] This approach is based on the discrete ordinate radiative transfer model introduced by Mudgett and Richards.[22] However, these methods yield numerical solutions rather than analytical solutions, making it difficult, generally, to obtain model parameters from the results of BRDF measurements.

A BRDF model is a reasonable strategy for approximating the BRDF of objects, and the parameters in the BRDF model are considered to be effective in representing the material characteristics of objects. A BRDF model is a mathematical model for BRDF, and it is able to fit to a BRDF sampled at sparse geometries. Typical BRDF models parameterize in terms of diffuse and specular reflection components, using parameters related with the sharpness or roughness of the specularity. Numerous BRDF models have been introduced, as summarized by Nayer.[23] In our previous study, we found that the TSL model,[24] which is a linear combination of two BRDF models: the Torrance-Sparrow model[25] for specular components, and the Lambert model[26] for diffuse components, gave good approximations for the BRDF of gold-coated paper sheets.

In the estimation of BRDF model parameters, it is significant to reduce the number of measurement geometries to achieve efficient characterization, as the measurement task of BRDF generally become more time-consuming and cumbersome as the number of reflectance measurements increase. Concerning the problem of importance sampling in BRDF measurements, an incremental method to minimize uncertainties in estimating BRDF model parameters was proposed by Lensch et al.[27] Techniques to estimate the appearance of an object from a sparse set of images were extensively reviewed in their study,[27] and are mainly based on an image-based method. The measurements in these studies were performed using a point light source[28–34] or by inverse global illumination.[35–39] However, contrary to the computational approaches listed above, the empirical approaches toward the problem are also considerable.

Measurement geometries in the specular reflection plane are important for the characterization of white paper sheets, as these geometries reveal a lot about the characteristic features of white paper sheets. In the case of glossy paper, a sharp, intense specular peak appears in the specular reflection plane. Paper with a fiber-containing surface also exhibits distinct forward scattering, which produces a large lobe in the BRDF at angles much larger than the specular reflection angle near the specular plane.[40] Trained forensic document examiners learn by experience that it is important to observe the luster of paper sheets under specular geometries to perceive the material characteristics of paper sheets. They also observe the intensity of diffuse reflected light under ordinary geometries, for example geometry 45/0, in order to make a contrast with the luster stated above.

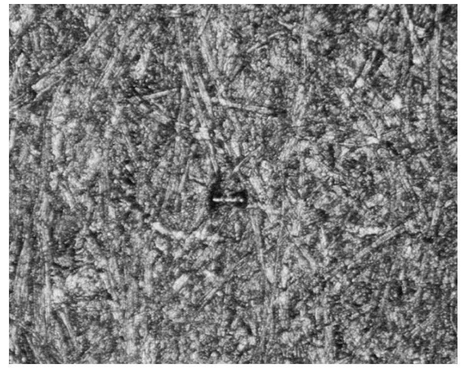

Figure 1. Microscopic observation of a paper for plain photocopies processed with gold evaporation.

Therefore in this study, we attempt to characterize white paper sheets using TSL model parameters estimated from the BRDF data in the specular reflection plane. Furthermore, we study an empirical strategy in reducing the number of measurement geometries and the feasibility of selecting geometries in the specular reflection plane in order to achieve an efficient characterization of white paper sheets.

TSL MODEL

In this study, the BRDF of samples was approximated using a linear combination of two BRDF models: the Torrance-Sparrow model[25] (TS model) and the Lambert model[26] (L model). We refer to this linear combination model as the TSL model. The TSL model is based on a dichromatic reflection model,[41] which expresses the BRDF as a linear combination of surface and body reflection components.

In our previous study, we found that the TSL model gave good approximations for measurements of gold-coated paper sheets.[24] Light reflected from paper sheets consists of a surface reflection component and a diffuse reflection component. The surface reflection component consists of light reflected only a few times from fibers near the surface, whereas the diffuse reflection component is from light randomly diffused by fibers within the paper sheet.

The TS model is considered to be suitable for paper sheets as the assumptions in the model are consistent with the structure of paper surfaces. One assumption of the TS model is that the surface consists of a collection of V-grooves. Figure 1 shows the microscopic observation of a paper for plain photocopies processed with gold evaporation. Microscopic observations of the surfaces of paper sheets reveal that they consist of tiny fibers that are randomly distributed and are intertwined with each other. Their appearance resembles an assembly of V-grooves randomly distributed in all azimuthal directions. The L model was introduced to represent homogeneous diffuse reflection properties, and it has been used as a model for the BRDF for approximating the BRDF of paper sheets.

Figure 2 shows a schematic of the geometrical parameters defining the illumination and observation directions.

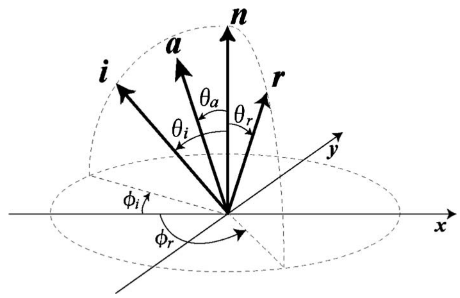

Figure 2. Schematic of geometrical parameters defining the illumination and observation directions.

The illumination direction is denoted by vector $\boldsymbol{i}$, the observation direction by $\boldsymbol{r}$, and the surface normal by $\boldsymbol{n}$. Vector $\boldsymbol{a}$ is the half vector between vectors $\boldsymbol{i}$ and $\boldsymbol{r}$. The illumination direction is represented by polar angle θ_i and azimuth angle ϕ_i. The observation direction is represented in the same manner as the incident direction by replacing suffix i with r.

The TSL model in the specular reflection plane is represented by

$$f_T(\theta_i,\theta_r) = \frac{\rho_s F(\psi) G(\theta_i,\theta_r)}{\cos(\theta_i)\cos(\theta_r)} \exp\left(-\frac{\theta_a^2}{2\sigma^2}\right) + \rho_d. \qquad (1)$$

The TSL model has four parameters: σ, ρ_s, ρ_d, and η. Parameter σ is the distribution of the V-groove facet angles defined in the TS model in terms of surface roughness, and ρ_s and ρ_d are the coefficients for the TS model and L model, respectively. $F(\psi)$ is the Fresnel coefficient given as follows,

$$F(\psi) = \sqrt{\left(\frac{\tan(\psi-\delta)}{\tan(\psi+\delta)}\right)^2 + \left(\frac{\sin(\psi-\delta)}{\sin(\psi+\delta)}\right)^2}, \qquad (2)$$

$$\psi = \frac{\theta_i+\theta_r}{2}, \quad \delta = \sin^{-1}\left(\frac{\sin\psi}{\eta}\right), \qquad (3)$$

where, η is the refractive index. $G(\theta_i,\theta_r)$ is the geometrical attenuation factor that expresses the shadowing and masking effects.[25] Blinn[42] gives a detailed description of this term, which may be summarized as

$$G(\theta_i,\theta_r) = \mathrm{Min}\left[1, \frac{2(\boldsymbol{n}\cdot\boldsymbol{a})(\boldsymbol{n}\cdot\boldsymbol{r})}{\boldsymbol{r}\cdot\boldsymbol{a}}, \frac{2(\boldsymbol{n}\cdot\boldsymbol{a})(\boldsymbol{n}\cdot\boldsymbol{i})}{\boldsymbol{r}\cdot\boldsymbol{a}}\right]. \qquad (4)$$

Geometrical variable θ_a is the angle between surface normal $\boldsymbol{n}$ and half vector $\boldsymbol{a}$.

MATERIALS AND METHODS

Samples for Analysis

Table I lists the specifications of the analysis samples. Eight types of paper sheets were analyzed. Glossy paper (G), semi-glossy paper (SG), matte coated paper (MC) and paper for plain photocopies (PPC) were the photocopy papers and printing papers. The Japanese papers (J1~J4) were traditional Japanese papers called *washi*, used for archiving documents in former times. They are currently used for calligraphy, and for arts and crafts. The Japanese papers were made from plant materials such as paper mulberries and *mitsumata*, which is a variety of daphne.

Table I. Specifications of the analysis samples.

Name	Specifications
G	Glossy paper (Seiko Epson, PMA4SP1)
SG	Semi-glossy paper (Seiko Epson, KA420MSH)
PPC	Paper for plain photocopies (NBS Ricoh, 90–1312)
MC	Matte coated paper (Seiko Epson, MJA4SP1)
J1	Japanese paper (Inaba Washi, Jyun-ganpi Momoyama)
J2	Japanese paper (Dai-insyu Paper Mill, C2.65kg)
J3	Japanese paper (Okamura Takao Paper Mill, Ranka)
J4	Japanese paper (Inaba Washi, No. 388)

The appearances of the analysis samples are shown in Figure 3. In this figure, each sample was in rounded shape in order to show its material characteristics such as roughness and glossiness. These samples had different material characteristics. Intense, sharp highlights were observed in sample G. They were also observed in sample SG, but their intensities were weaker and their widths were broader than those of the glossy paper. Gloss was not observed in samples PPC and MC. The surfaces of samples J1~J4 were generally rough and no coated materials were observed under microscopic observation. A slight gloss was observed in samples J1 and J2, but no gloss was seen in samples J3 and J4.

Each sample measured 60 mm by 150 mm. Although some printed lines and characters are seen on the paper sheets in Fig. 3, measurements were performed on areas in which there were no such lines and characters.

Measurement of Gonioreflection Properties in the Specular Reflection Plane

The gonioreflection properties of the samples were measured at the geometries in the specular reflection plane. We used a goniospectrophotometer (Murakami Color Research Laboratory, GCMS-4) for the measurements. Measurement geometries are listed in Table II. We took measurements at 284 geometries, which is the combination of four illumination directions and 71 observation directions. Each geometry is in the specular reflection plane.

For each geometry, spectral radiance was measured for wavelengths from 390 to 730 nm at 10 nm intervals. Y values were calculated from spectral radiance factors under the condition of D50 illuminant and CIE 1931 10° standard ob-

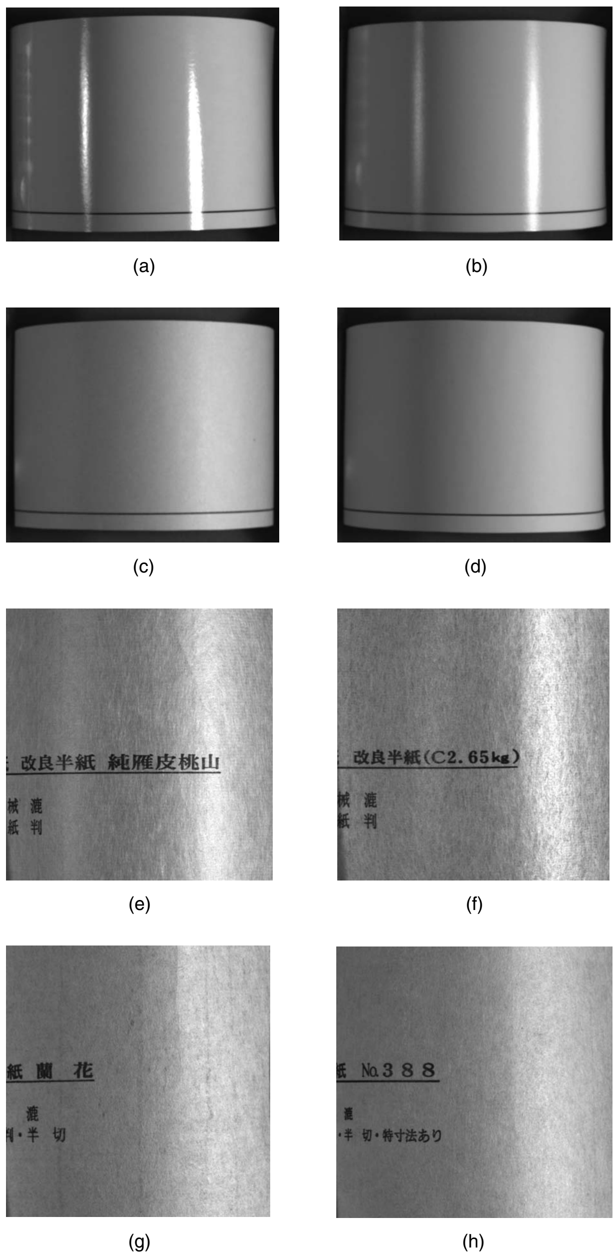

Figure 3. The appearances of the analysis samples: (a) G, (b) SG, (c) PPC, (d) MC, (e) J1, (f) J2, (g) J3 and (h) J4.

server. Radiance factors were calculated from the Y values by normalizing with the data for a perfect diffuser (i.e., $Y=100$).

Characterization by TSL Model Parameters

We characterized the material characteristics of white paper sheets using TSL model parameters, which were estimated from the radiance factors of the samples in the specular reflection plane. The radiance factors can be approximated by the BRDF model as they are equal to the BRDF normalized by a constant ($=1/\pi$), which is the BRDF of a perfect diffuser.

The TSL model parameters were estimated to minimize the Euclidean norm between the measured value and TSL model approximation. The estimation was performed by using the nonlinear optimization function "*fmincon*"[43] in numerical calculation software (MATHWORKS, MATLAB 6.0). This function finds minimum of constrained nonlinear multivariable function. The lower and upper bounds of each parameter were set as listed in Table III.

Table II. Geometries for BRDF measurements.

Illumination (4 directions)		Observation (71 directions)	
θ_i [deg]	ϕ_i [deg]	θ_r [deg]	ϕ_r [deg]
20			
30	0	$0 \sim 70$	180
45		$(\Delta 1)$	
60			

Table III. Lower and upper bounds of TSL model parameters in estimation.

Parameter	Lower bound	Upper bound
σ [deg]	0	90
ρ_s	0	∞
ρ_d	0	∞
η	1	3

The deviation between the TSL model approximation and the measurement value was evaluated by observing the data plotted against observation angle θ_r for each incident angle θ_i. The deviation was also numerically evaluated by normalized mean absolute error (NMAE). NMAE E_n is expressed as follows

$$E_n = \frac{E}{\max[f_m(\boldsymbol{r};\boldsymbol{i})] - \min[f_m(\boldsymbol{r};\boldsymbol{i})]}, \tag{5}$$

where $f_m(\boldsymbol{r};\boldsymbol{i})$ is the measurement value, E is the mean absolute error (MAE) given by

$$E = \frac{\sum_{r;i}^{N} |f_a(\boldsymbol{r};\boldsymbol{i}) - f_m(\boldsymbol{r};\boldsymbol{i})|}{N}, \tag{6}$$

where $f_a(\boldsymbol{r};\boldsymbol{i})$ is the approximated value, N is the number of measurement geometries. In this study, $N=284$. The reason we used NMAE and not the Euclidean norm was the significant difference in dynamic range among the samples. By normalizing the range of the radiance factor of each sample, we evaluated the precision uniformly among the different types of paper sheets.

Parameter Estimation from Geometrically Sparse Data

We reduced the number of measurement geometries for parameter estimation using the following two strategies. In each strategy, the number of observation directions was reduced.

Table IV. Measurement geometries for Strategy 1 of the parameter estimation from geometrically sparse data.

Number of geometries M	δ [deg]	θ_i [deg]	θ_r [deg]																
12	35	20	0				20												70
		30	0							30									70
		45	0										45						70
		60	0													60			70
16	24	20	0				20						45						70
		30	0							30				50					70
		45	0					23					45						70
		60	0							30						60			70
20	18	20	0				20				37				53				70
		30	0			15				30				50					70
		45	0					23					45		58				70
		60	0				20					40				60			70
24	14	20	0				20				33		45		58				70
		30	0			15				30		43			57				70
		45	0					~Δ15~					45		57				70
		60	0						~Δ15~							60			70
36	9	20	0		10		20		28		37		45		54			62	70
		30	0		10		20			30	38			46	54			62	70
		45	0					~Δ9~					45	53				62	70
		60	0	8		17		25			34	42		51		60			70
60	5	20	0		~Δ5~		20						~Δ5~						70
		30	0				~Δ5~			30					~Δ5~				70
		45	0					~Δ5~					45			~Δ5~			70
		60	0							~Δ5~						60		65	70
76	4	20	0		~Δ4~		20						~Δ4~					68	70
		30	0	4	8	13	17	21	26	30	32				~Δ4~			68	70
		45	0					~Δ4~				40	45	48		~Δ4~		68	70
		60	0							~Δ4~						60	64	68	70
144	2	20	0		~Δ2~		20						~Δ2~						70
		30	0				~Δ2~			30					~Δ2~				70
		45	0					~Δ2~				42	45	46		~Δ2~			70
		60	0							~Δ2~						60	~Δ2~		70

Strategy1: Constant Distribution of Observation Directions

In the first strategy, we reduced the number of observation directions at a constant interval. The measurement geometries for Strategy 1 are listed in Table IV. We tried eight conditions, in which the number of selected geometries M was 12, 16, 20, 24, 36, 60, 76, and 144. The intervals for observation direction δ were 35°, 24°, 18°, 14°, 9°, 5°, 4°, and 2°, respectively. The observation directions were decreased at a constant interval.

In each selection, the following three observation directions were included, surface normal direction ($\theta_r=0$), specular reflection direction ($\theta_r=\theta_i$), and maximum of θ_r ($\theta_r=70$). According to the increase in sampling geometries, a new sampling geometry was added by dividing equally the largest section of θ_r.

Strategy 2: Dense Distribution Only around Specular Directions

In the second strategy, we reduced the number of geometries by distributing observation geometries densely only around specular directions. Measurement geometries for Strategy 2 are listed in Table V. We tried ten conditions in which the interval of observation direction δ was from 1° to 10°. The

Table V. Measurement geometries for Strategy 2 of the parameter estimation from geometrically sparse data.

Number of geometries M	δ [deg]	θ_i [deg]	θ_r [deg]										
19	10	20	0	10		20		30					70
		30	0			20		30		40			70
		45	0					35		45		55	70
		60	0							50		60	70
26	9	20	0	2	$\sim\Delta 9\sim$	20	$\sim\Delta 9\sim$	38					70
		30	0			12	$\sim\Delta 9\sim$	30	$\sim\Delta 9\sim$	48			70
		45	0					27	$\sim\Delta 9\sim$	45	$\sim\Delta 9\sim$	63	70
		60	0							42	$\sim\Delta 9\sim$	60	69
26	8	20	0	4	$\sim\Delta 8\sim$	20	$\sim\Delta 8\sim$	36					70
		30	0			14	$\sim\Delta 8\sim$	30	$\sim\Delta 8\sim$	46			70
		45	0					29	$\sim\Delta 8\sim$	45	$\sim\Delta 8\sim$	61	70
		60	0							44	$\sim\Delta 8\sim$	60	68
26	7	20	0	6	$\sim\Delta 7\sim$	20	$\sim\Delta 7\sim$	34					70
		30	0			26	$\sim\Delta 7\sim$	30	$\sim\Delta 7\sim$	44			70
		45	0					31	$\sim\Delta 7\sim$	45	$\sim\Delta 7\sim$	59	70
		60	0							46	$\sim\Delta 7\sim$	60	67
26	6	20	0	8	$\sim\Delta 6\sim$	20	$\sim\Delta 6\sim$	32					70
		30	0			18	$\sim\Delta 6\sim$	30	$\sim\Delta 6\sim$	42			70
		45	0					33	$\sim\Delta 6\sim$	45	$\sim\Delta 6\sim$	58	70
		60	0							46	$\sim\Delta 6\sim$	60	66
27	5	20	0	10	$\sim\Delta 5\sim$	20	$\sim\Delta 5\sim$	30					70
		30	0			20	$\sim\Delta 5\sim$	30	$\sim\Delta 5\sim$	40			70
		45	0					35	$\sim\Delta 5\sim$	45	$\sim\Delta 5\sim$	55	70
		60	0							50	$\sim\Delta 5\sim$	60	$\sim\Delta 5\sim$ 70
34	4	20	0	8	$\sim\Delta 4\sim$	20	$\sim\Delta 4\sim$	32					70
		30	0			18	$\sim\Delta 4\sim$	30	$\sim\Delta 4\sim$	42			70
		45	0					33	$\sim\Delta 4\sim$	45	$\sim\Delta 4\sim$	57	70
		60	0							48	$\sim\Delta 4\sim$	60	$\sim\Delta 4\sim$ 68
42	3	20	0	8	$\sim\Delta 3\sim$	20	$\sim\Delta 3\sim$	32					70
		30	0			18	$\sim\Delta 3\sim$	30	$\sim\Delta 3\sim$	42			70
		45	0					33	$\sim\Delta 3\sim$	45	$\sim\Delta 3\sim$	57	70
		60	0							48	$\sim\Delta 3\sim$	60	$\sim\Delta 3\sim$ 69
51	2	20	0	10	$\sim\Delta 2\sim$	20	$\sim\Delta 2\sim$	30					70
		30	0			20	$\sim\Delta 2\sim$	30	$\sim\Delta 2\sim$	40			70
		45	0					35	$\sim\Delta 2\sim$	45	$\sim\Delta 2\sim$	55	70
		60	0							50	$\sim\Delta 2\sim$	60	$\sim\Delta 2\sim$ 70
91	1	20	0	10	$\sim\Delta 1\sim$	20	$\sim\Delta 1\sim$	30					70
		30	0			20	$\sim\Delta 1\sim$	30	$\sim\Delta 1\sim$	40			70
		45	0					35	$\sim\Delta 1\sim$	45	$\sim\Delta 1\sim$	55	70
		60	0							50	$\sim\Delta 1\sim$	60	$\sim\Delta 1\sim$ 70

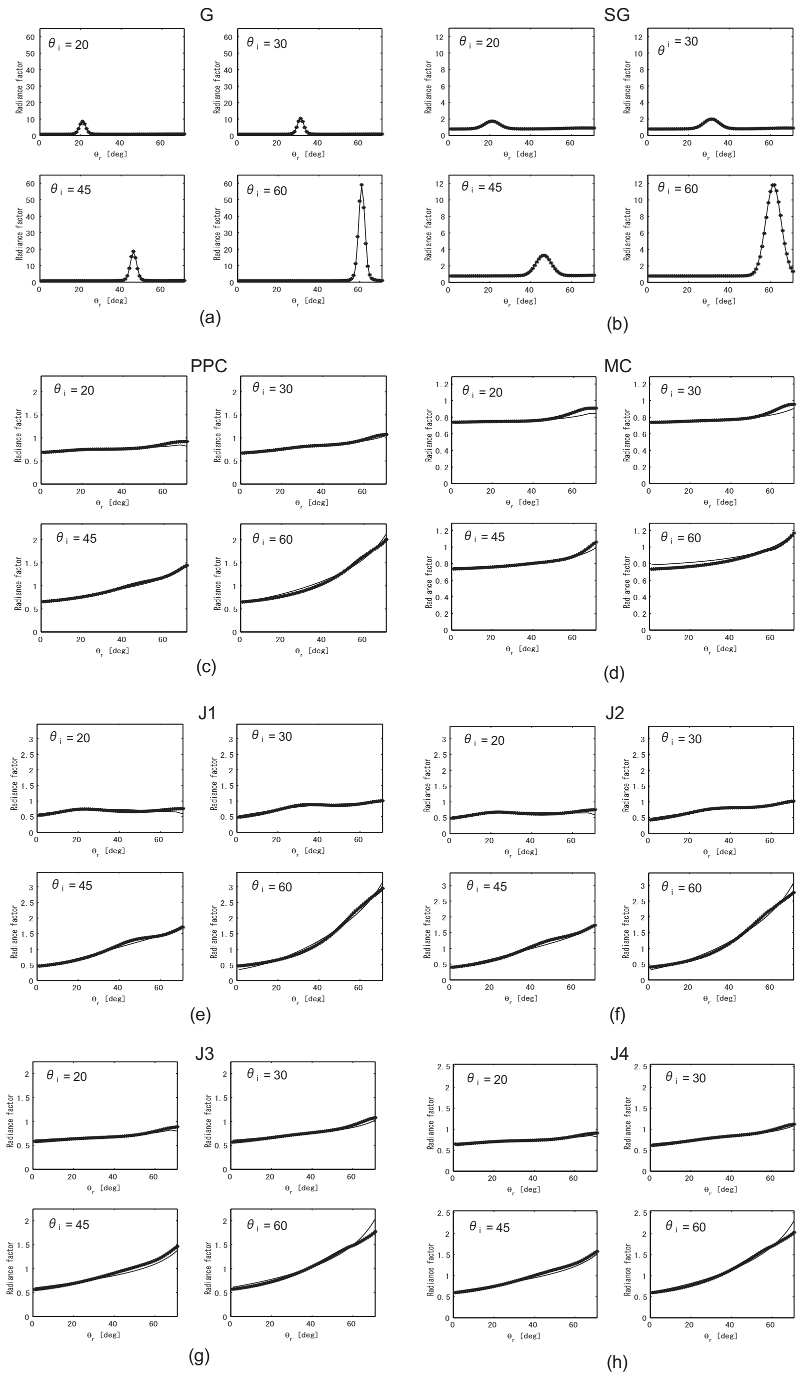

Figure 4. Radiance factor of each sample (asterisks) and its approximation by the TSL model (solid lines): (a) G, (b) SG, (c) PPC, (d) MC, (e) J1, (f) J2, (g) J3 and (h) J4.

range of dense observation directions was from $-10°$ to $10°$ around the specular directions. In each selection, three types of conditions concerning observation directions ($\theta_r = 0°$, θ_i and $70°$) were included. However the condition $(\theta_i, \theta_r) = (60, 70)$ was not included where δ is not a divisor of 10.

RESULTS AND DISCUSSION

Gonioreflection Properties in the Specular Reflection Plane

The gonioreflection properties in the specular plane were different among the samples. Figure 4 shows the measurement results and TSL model approximation of the radiance factor of each sample. There are four graphs, corresponding to each sample. These four graphs correspond to each incident angle θ_i. In each graph, the radiance factor is plotted against the reflection angle θ_r. Asterisks represent the measured values, and the solid lines indicate the TSL model approximation.

With glossy papers (G and SG), mirrorlike reflections with intense and sharp peaks were observed in specular geometries. The specular peaks of SG were weaker and broader than those of G. Specular peaks became stronger as incident

Table VI. TSL model parameters of each sample estimated from BRDF in the specular reflection plane.

Sample	σ [deg]	ρ_s	ρ_d	η
G	0.8	57.8	0.855	1.19
SG	1.9	57.1	0.795	1.02
PPC	21.7	0.409	0.414	3.00
MC	43.5	0.123	0.642	3.00
J1	16.7	0.734	0.127	3.00
J2	17.9	0.729	0.060	3.00
J3	24.5	0.404	0.333	3.00
J4	21.9	0.469	0.346	3.00

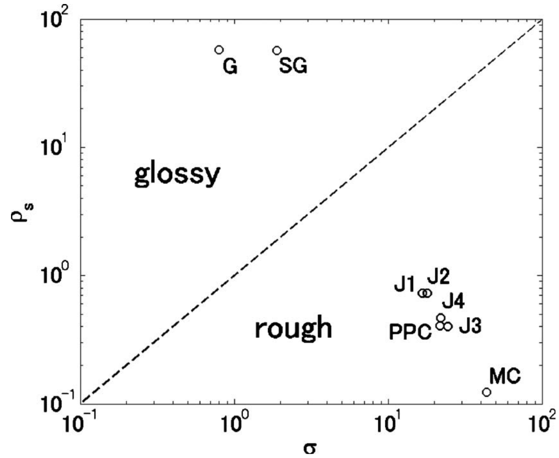

Figure 5. TSL model parameter plots of the analysis samples in σ-ρ_s plane.

angle θ_i increased. Constant diffuse reflection was observed, except in specular geometries.

For rough papers (PPC, MC, J1, J2, J3, and J4), the radiance factor increased as observation angle θ_r increased. This tendency became more extreme in line with an increase in the incident angle θ_i. The degree of this tendency was different among the groups. The first group was PPC, J3, and J4. The second group was J1 and J2. In the second group, the radiance factor increased slightly around the specular reflection geometries, however, this characteristic was not pronounced in the case of large incident angles, such as $\theta_i=60°$. The third sample, sample MC, showed an almost constant Lambertian-like diffuse reflection concurrently with a slight increase in the radiance factor as observation angle θ_r increased.

Approximation by the TSL Model

As seen from Fig. 4, the gonioreflection properties of each sample in the specular reflection planes were approximated very well by the TSL model. The mirrorlike reflections at specular geometries in the glossy samples were predicted. The width and height of the specular reflections were also estimated accurately. In the rough samples, a gradual increase of the radiance factor, in line with the increase of observation angle θ_r was approximated very well. However in J1 and J2, the slight increase in the radiance factor around the specular geometries was not represented.

The NMAE between the TSL model approximation and the measurement value was less than 4.5% for each sample. It is considered that the reason for the excellent approximation results was mainly due to the high capability of the TS model.

Characterization by TSL Model Parameters

The estimated TSL model parameters of each sample are shown in Table VI. As the sample becomes glossy, roughness parameter σ decreased and TS model coefficient ρ_s increased. In the rough samples (PPC, MC, J1, J2, J3, and J4), TS model coefficient ρ_s increased and L model coefficient ρ_d decreased as samples become glossier. Between two glossy samples (G and SG), there was a difference in roughness parameter σ.

Concerning parameter η, which is refractive index used to calculate the Fresnel index in the TS model, the estimated value was three for all six rough samples. The value $\eta=3$ was the upper limit for the parameter search space in this study. The gonioproperties of the Fresnel term becomes insignificant in line with the increase in the refractive index. The approximation may be improved if the refractive index η is allowed to be larger than three. However, a refractive index much larger than three would be unrealistic. The problems of the Fresnel term for rough paper sheets were not considered owing to the limits of the TS model, and this remains a task for future work.

Classification between Glossy and Rough Samples

Classification between glossy paper and rough samples was performed by the parameter plots in the σ-ρ_s plane as shown in Figure 5. Based on the threshold $\sigma=\rho_s$, samples were clearly classified into glossy samples (G and SG: $\sigma<\rho_s$) and rough samples (PPC, MC, J1, J2, J3, and J4: $\sigma>\rho_s$).

This metric was also available in the case of parameter estimation from geometrically sparse data. The parameter plots in the σ-ρ_s plane in the case of Strategy 1 and Strategy 2 are shown in Figures 6(a) and 6(b), respectively. The parameters in all cases listed in Tables IV and V are plotted together on each figure. Samples were successfully classified in all cases for each strategy, even in the case of the smallest number of geometries, with observation direction intervals of $\delta=35°$ and 10° for each strategy.

Classification of Rough Samples

Classification of rough samples (PPC, MC, J1, J2, J3, and J4) was performed by the parameter plots in the ρ_s-ρ_d plane as shown in Figure 7. Rough samples were clearly classified into three groups: (I) Japanese papers with a slight gloss (J1 and J2: $\rho_d/\rho_s<1/2.53$), (II) PPC paper or Japanese papers without gloss (PPC, J3 and J4: $1/2.53\leq\rho_d/\rho_s<1.83$) and (III) matte coated paper (MC: $1.83\leq\rho_d/\rho_s$).

This metric was also available in the case of parameter estimation from geometrically sparse data. The parameter

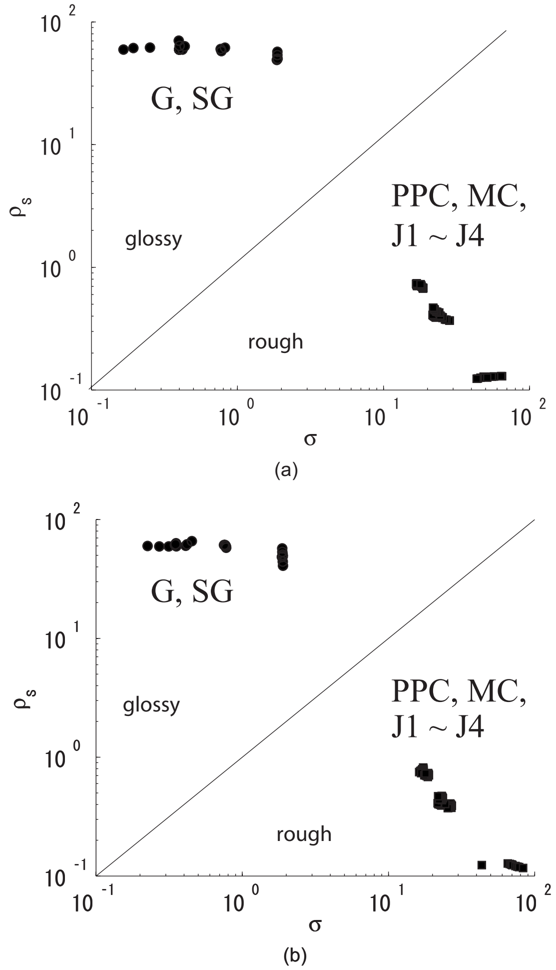

Figure 6. TSL model parameter plots of the analysis samples in σ-ρ_s plane in the case of parameter estimation from geometrically sparse data: (a) Strategy 1 and (b) Strategy 2.

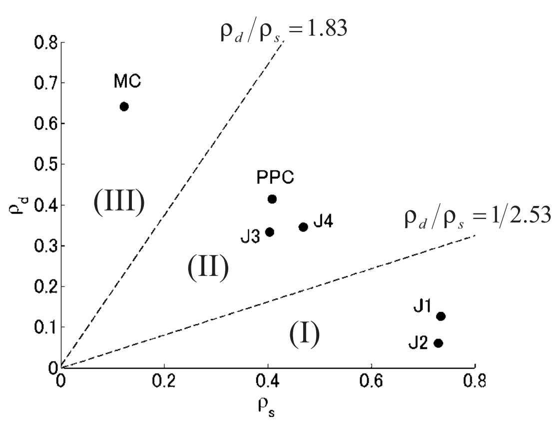

Figure 7. TSL model parameter plots of rough paper samples in ρ_s-ρ_d plane.

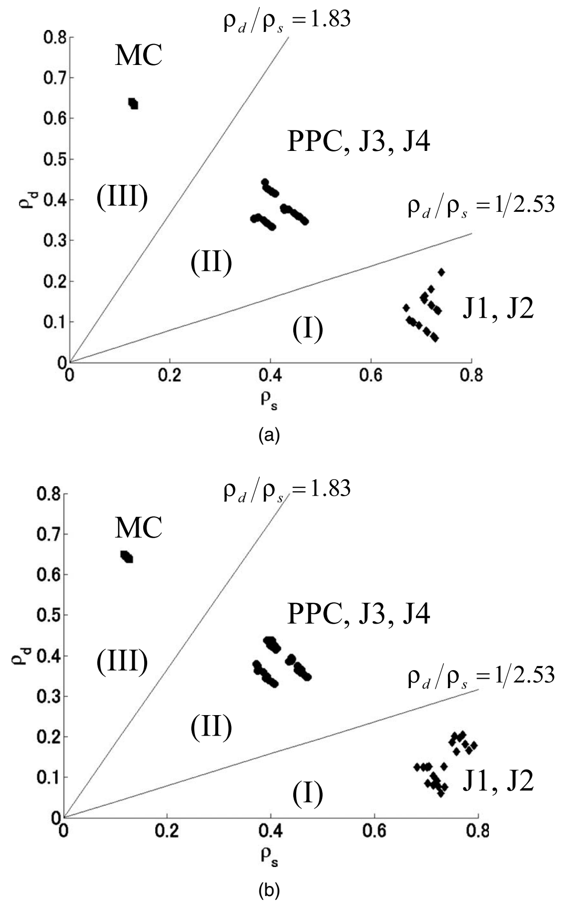

Figure 8. TSL model parameter plots of rough paper samples in ρ_s-ρ_d plane in the case of parameter estimation from geometrically sparse data: (a) Strategy 1 and (b) Strategy 2.

plots in the ρ_s-ρ_d plane in the case of Strategy 1 and Strategy 2 are shown in Figures 8(a) and 8(b), respectively. The parameters in all cases listed in Tables IV and V are plotted together on each figure. Samples were successfully classified in all cases of each strategy, even in the case of the smallest number of geometries, with observation direction intervals of δ=35° and 10° for each strategy.

Classification of Glossy Samples

We characterized two glossy papers (G and SG) based on roughness parameter σ. Table VI shows parameter σ for G and SG was 0.8 and 1.9, respectively. However for shiny materials, the BRDF contains significant high-frequency components, and parameters obtained by fitting to a limited number of samples may mischaracterize the specular behavior of the material.

Figures 9(a) and 9(b) show roughness parameter σ plotted against the interval of observation direction δ for each strategy. The results are shown for glossy paper (G) and semi-glossy paper (SG). The value assigned to the parameter σ is highly dependent on δ. The background to this issue is considered to be the problem of the sharp specular peak existing in glossy papers. In order to estimate proper BRDF model parameters, it is important to detect the shape of the specular peak. In general, the width of the specular peak is narrow, and the full width at half maximum (FWHM) of the specular peak was 4.3° in sample G, and 9.8° in sample SG. Therefore, it is difficult to detect the peak shape with sampling intervals that are broader than the peak width. In every condition of measurement geometries in which TSL model

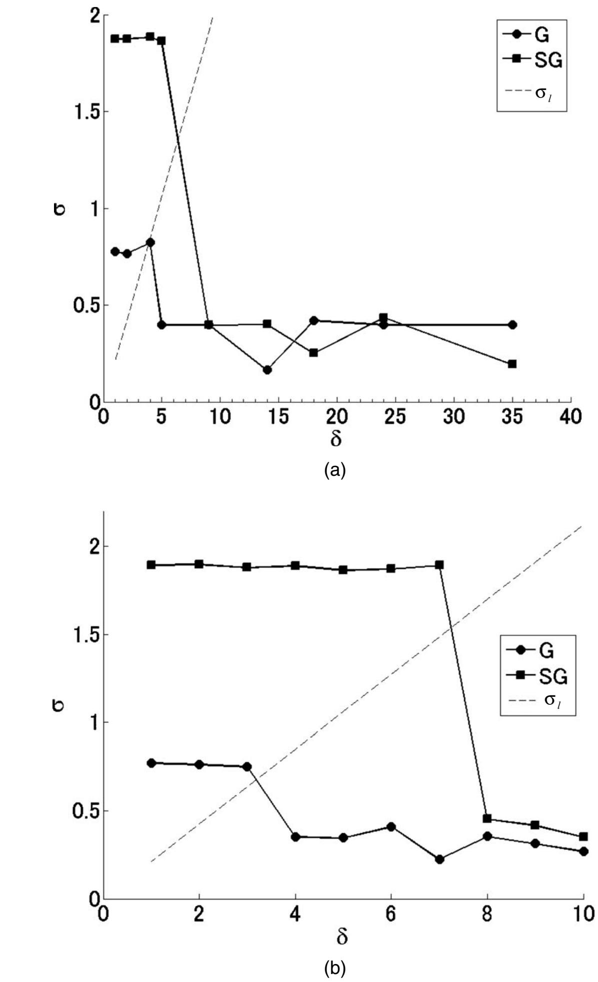

Figure 9. The roughness parameter σ of glossy paper (G) and semi-glossy paper (SG) plotted against the interval of observation direction δ: (a) Strategy 1 and (b) Strategy 2. The dashed plots shows the value σ_l, which gives the FWHM of the specular peak in the TS model equal to sampling interval δ.

parameters were properly estimated in this study, the interval of observation direction around the specular peak was smaller than the FWHM of the specular peak.

The dashed plot in Figs. 9(a) and 9(b) shows parameter σ, which gives the FWHM of the specular peak in the TS model equal to sampling interval δ. In this study we call parameter σ in such a condition σ_l. The value of σ_l is represented as follows:

$$\sigma_l = \frac{\delta}{4\sqrt{2}\ln 2}. \tag{7}$$

As seen from Fig. 9, the parameter σ was correctly estimated under the condition $\sigma > \sigma_l$. In other words, if estimated parameter σ is smaller than σ_l, the estimated parameter may contain errors. This metric is one of the criteria by which to judge proper parameter estimation.

Classification Metrics for White Paper Sheets

In summary, the proposed classification metrics for white paper sheets in this study are shown in Figure 10.

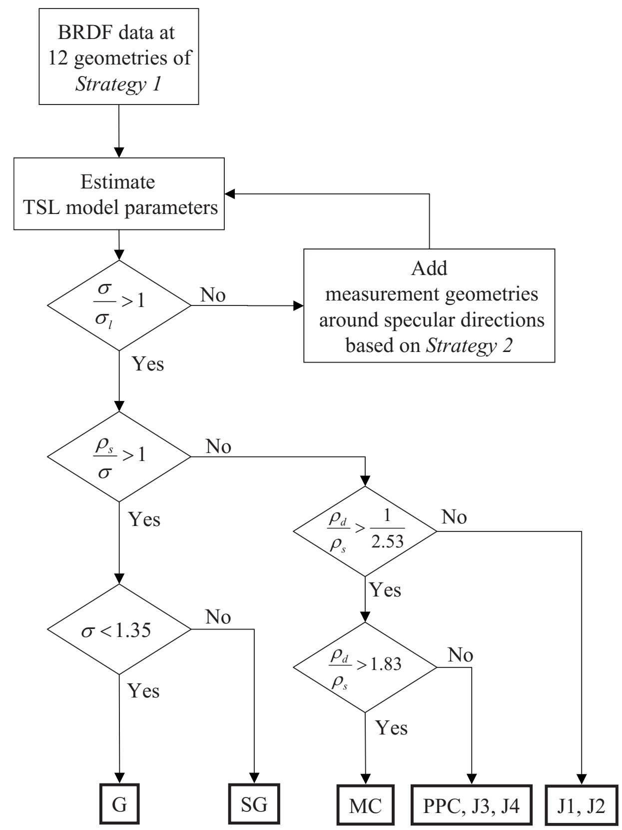

Figure 10. Classification metrics for white paper sheets in this study.

First, parameter estimation is performed using data taken at 12 geometries of Strategy 1. In the first step, the appropriateness of estimated parameter σ is evaluated using the metric $\sigma > \sigma_l$. If the condition is not satisfied, the number of the measurement geometry is added based on Strategy 2, and parameter estimation is performed.

Using the estimated parameters, classification between glossy and rough samples can be performed. If the sample is classified into the glossy group, classification between sample G and SG is performed based on parameter σ. If the sample is classified into the rough group, further classification is performed based on parameters ρ_s and ρ_d.

In future work, a further reduction of measurement geometries is required for more efficient and practical characterization. However, there are many other combinations to extract a small number of geometries from the total 284 geometries. Adaptive positioning of measurement geometries according to the gonioreflection properties of paper samples remains a challenging problem for future work.

CONCLUSIONS

We proposed a characterization metric for white paper sheets based on TSL model parameters. Efficient characterization was achieved by model parameter estimation from a small BRDF number at sparse geometries in the specular reflection plane. Eight sheets of white paper were properly classified into five groups by using the two criteria successively. The first criterion classified the samples into two (glossy or rough) groups. The second criterion classified rough paper samples into three groups. Glossy papers were characterized by a roughness parameter in the TS model. The model parameters required for the first classification were estimated from the BRDF data at 12 geometries. The parameters estimated for the first classification were effective for the second classification of rough paper samples. The roughness parameters used for the characterization of glossy papers should be estimated from the BRDF data sampled at a smaller interval than the FWHM of the specular peak. It proved an effective strategy to distribute measurement geometries densely only around the specular direction for efficient model parameter estimation. In summary, the proposed method was considered an efficient characterization metric for white paper sheets in a wide range of material characteristics.

REFERENCES

[1] ISO 11476:2000 Paper and board—Determination of CIE-whiteness, C/2 degree (indoor illumination conditions).

[2] ISO 2471:2008 Paper and board—Determination of opacity (paper backing)—Diffuse reflectance method.

[3] ISO 5631–1:2009 Paper and board—Determination of colour by diffuse reflectance—Part 1: Indoor daylight conditions (C/2 degrees).

[4] ISO 5631–2:2008 Paper and board—Determination of colour by diffuse reflectance—Part 2: Outdoor daylight conditions (D65/10 degrees).

[5] ISO 5631–3:2008 Paper and board—Determination of colour by diffuse reflectance—Part 3: Indoor illumination conditions (D50/2 degrees).

[6] ISO 2470–1:2009 Paper, board and pulps—Measurement of diffuse blue reflectance factor—Part 1: Indoor daylight conditions (ISO brightness).

[7] ISO 2470–2:2008 Paper, board and pulps—Measurement of diffuse blue reflectance factor—Part 2: Outdoor daylight conditions (D65 brightness).

[8] ISO 9416:2009 Paper—Determination of light scattering and absorption coefficients (using Kubelka-Munk theory).

[9] ISO 8254–1:2009 Paper and board—Measurement of specular gloss—Part 1: 75 degree gloss with a converging beam, TAPPI method.

[10] ISO 8254–2:2003 Paper and board—Measurement of specular gloss—Part 2: 75 degree gloss with a parallel beam, DIN method.

[11] ISO 8254–3:2004 Paper and board—Measurement of specular gloss—Part 3: 20 degree gloss with a converging beam, TAPPI method.

[12] H. Lipshitz, M. Bridger, and G. Derman, "On the relationships between topography and gloss", Tappi J. **73**, 237 (1990).

[13] S. Serikawa and T. Shimomura, "Method for measuring glossiness of plane surfaces based on psychological sensory scale", IEICE Trans. Fundamentals **E76-A**, 439 (1993).

[14] S. Serikawa and T. Shimomura, "Extraction of glossiness of curved surfaces by the use of spatial filter simulating retina function", IEICE Trans. Inf. Syst. **E77-D**, 335 (1994).

[15] F. E. Nicodemus, "Reflectance nomenclature and directional reflectance and emissivity", Appl. Opt. **9**, 1474 (1970).

[16] P. Kubelka and F. Munk, "Ein Beitrag zur Optik der Farbenstriche", Z. Tech. Phys. (Leipzig) **12**, 593 (1931) (In German).

[17] P. Kubelka, "New contribution to the optics of intensely light-scattering materials. Part I", J. Opt. Soc. Am. **38**, 448 (1948).

[18] S. Chandrasekhar, *Radiative Transfer* (Dover Publications, New York, 1960).

[19] L. G. Henyey and J. L. Greenstein, "Diffuse radiation in the galaxy", Astrophys. J. **93**, 70 (1941).

[20] P. Edström, *Fast and stable solution method for angular-resolved light scattering simulation*, Internal FSCN report: R-02–35, Mid Sweden University, Sweden, 2002.

[21] H. Granberg and P. Edström, "Quantification of the intrinsic error of Kubelka-Munk model caused by strong light absorption", J. Pulp Pap. Sci. **29**, 386 (2003).

[22] P. Mudgett and L. W. Richards, "Multiple scattering calculation for technology", Appl. Opt. **10**, 1485 (1971).

[23] S. K. Nayar, K. Ikeuchi, and T. Kanade, "Surface reflection: physical and geometrical perspectives", IEEE Trans. Pattern Anal. Mach. Intell. **13**, 611 (1991).

[24] Y. Akao, N. Tsumura, T. Nakaguchi, and Y. Miyake, "Approximation of the gonio radiance properties of gold-coated paper sheets by BRDF models", Jpn. J. Forensic Sci. Tech. **12**, 107 (2007) (in Japanese).

[25] K. E. Torrance and E. M. Sparrow, "Theory for off-specular reflection from roughened surfaces", J. Opt. Soc. Am. **57**, 1105 (1967).

[26] J. Lambert, *Photometria Sive de Mensure de Gratibus Luminis, Colorum Umbrae* (Eberhard Klett, Augsberg, Germany, 1760) (In Latin).

[27] H. P. A. Lensch, J. Lang, A. M. Sá, and H.-P. Seidel, "Planned sampling of spatially varying BRDFs", Comput. Graph. Forum **22**, 473 (2003).

[28] H. P. A. Lensch, J. Kautz, M. Goesele, W. Heidrich, and H.-P. Seidel, "Image-based reconstruction of spatially varying materials", *12th Eurographics Workshop on Rendering* (Springer, Wien, 2001) pp. 103–114.

[29] H. P. A. Lensch, J. Kautz, M. Goesele, W. Heidrich, and H.-P. Seidel, "Image-based reconstruction of spatial appearance and geometric detail", ACM Trans. Graphics **22**, 234 (2003).

[30] Y. Li, S. Lin, S. B. Kang, H. Lu, and H.-Y. Shum, "Single-image reflectance estimation for relighting by iterative soft grouping", *Pacific Graphics '02* (IEEE, Washington, DC, 2002) pp. 483–486.

[31] S. Marschner, B. Guenter, and S. Raghupathy, "Modeling and rendering for realistic facial animation", *11th Eurographics Workshop on Rendering* (Springer, Wien, 2000) pp. 231–242.

[32] S. Marschner, S. Westin, E. Lafortune, K. Torrance, and D. Greenberg, "Image-based BRDF measurement including human skin", *10th Eurographics Workshop on Rendering* (Springer, Wien, 1999) pp. 131–144.

[33] K. Nishino, Y. Sato, and K. Ikeuchi, "Eigen-texture method: Appearance compression and synthesis based on a 3D model", IEEE Trans. Pattern Anal. Mach. Intell. **23**, 1257 (2001).

[34] Y. Sato, M. Wheeler, and K. Ikeuchi, "Object shape and reflectance modeling from observation", *Computer Graphics Proceedings, Annual Conference Series 1997, ACM SIGGRAPH* (ACM, New York, 1997) pp. 379–387.

[35] S. Boivin and A. Gagalowicz, "Image-based rendering of diffuse, specular and glossy surfaces from a single image", *Computer Graphics Proceedings, Annual Conference Series, ACM SIGGRAPH* (ACM, New York, 2001) pp. 107–116.

[36] S. Gibson, T. Howard, and R. Hubbold, "Flexible image-based photometric reconstruction using virtual light sources", Comput. Graph. Forum **20**, 203 (2001).

[37] K. Nishino, Z. Zhang, and K. Ikeuchi, "Determining reflectance parameters and illumination distribution from a sparse set of images for view-dependent image synthesis", *Proc. Eighth IEEE International Conference on Computer Vision (ICCV '01)* (IEEE, Piscataway, NJ, 2001) Vol. **1**, pp.599–606.

[38] R. Ramamoorthi and P. Hanrahan, "A signal-processing framework for inverse rendering", *Computer Graphics Proceedings, Annual Conference Series ACM SIGGRAPH* (ACM, New York, 2001) pp. 117–128.

[39] Y. Yu and J. Malik, "Recovering photometric properties of architectural scenes from photographs", *Computer Graphics Proceedings, Annual Conference Series, ACM SIGGRAPH* (ACM, New York, 1998) pp. 207–217.

[40] H. Granberg, J. Jensen, and L. Mattsson, "Forward scattering of fiber-containing surfaces studied by 3-D reflectance distribution simulationsand measurements", Opt. Eng. **42**, 2384 (2003).

[41] S. A. Shafer, "Using color to separate reflection components", Color Res. Appl. **10**, 210 (1985).

[42] J. Blinn, "Models of light reflection for computer synthesized pictures", Comput. Graph. (ACM) **11**, 192 (1977).

[43] Find minimum of constrained nonlinear multivariable function—MATLAB, The MathWorks, http://www.mathworks.com/access/helpdesk/help/toolbox/optim/ug/fmincon.html, accessed April 2010.